

Unsupervised Learning on Neural Network Outputs

Yao Lu

University of Helsinki

Aalto University

Helsinki Institute for Information Technology

yaolubrain@gmail.com

Abstract

The outputs of a trained neural network contain much richer information than just an one-hot classifier. For example, a neural network might give an image of a dog the probability of one in a million of being a cat but it is still much larger than the probability of being a car. To reveal the hidden structure in them, we apply two unsupervised learning algorithms, PCA and ICA, to the outputs of a deep Convolutional Neural Network trained on the ImageNet of 1000 classes. The PCA/ICA embedding of the object classes reveals their visual similarity and the PCA/ICA components can be interpreted as common visual features shared by similar object classes. For an application, we proposed a new zero-shot learning method, in which the visual features learned by PCA/ICA are employed. Our zero-shot learning method achieves the state-of-the-art results on the ImageNet of over 20000 classes.

1. Introduction

Recently, Convolutional Neural Network (CNN) [25] has made significant advances in computer vision tasks such as image classification [7, 22, 35], object detection [14, 32] and image segmentation [36, 26]. Moreover, CNN also sheds lights on neural coding in visual cortex. In [6], it has been shown that a trained CNN rivals the representational performance of inferior temporal cortex on a visual object recognition task. Therefore, investigating the properties of a trained CNN is important for both computer vision applications and discovering the principles of neural coding in the brain.

In [16], Hinton et al. showed that the softmax outputs of a trained neural network contain much richer information than just a one-hot classifier. Such a phenomenon is called *dark knowledge*. For input vector $\mathbf{y} = (y_1, \dots, y_n)$, which is called logits in [16], the softmax function produces output

vector $\mathbf{x} = (x_1, \dots, x_n)$ such that

$$x_i = \frac{\exp(y_i/T)}{\sum_j \exp(y_j/T)} \quad (1)$$

where T is the temperature parameter. The softmax function assigns positive probabilities to all classes since $x_i > 0$ for all i . Given a data point of a certain class as input, even when the probabilities of the incorrect classes are small, some of them are much larger than the others. For example, in a 4-class classification task (cow, dog, cat, car), given an image of a dog, while a hard target (class label) is $(0, 1, 0, 0)$, a trained neural network might output a soft target $(10^{-6}, 0.9, 0.1, 10^{-9})$. An image of a dog might have small chance to be misclassified as cat but it is much less likely to be misclassified as car. In [16], a technique called knowledge distillation was introduced to further reveal the information in the softmax outputs. Knowledge distillation raises the temperature T in the softmax function to soften the outputs. For example, it transforms $(10^{-6}, 0.9, 0.1, 10^{-9})$ to $(0.015, 0.664, 0.319, 0.001)$ by raising temperature T from 1 to 3. It has been shown that adding the distilled soft targets in the objective function helps in reducing generalization error when training a smaller model of an ensemble of models [16]. Therefore, the outputs of a trained neural network are far from one-hot hard targets or random noise and they might contain rich statistical structures.

In this paper, to explore the information hidden in the outputs, we apply two unsupervised learning algorithms, Principle Component Analysis (PCA) and Independent Component Analysis (ICA) to the outputs of a CNN trained on the ImageNet dataset [8] of 1000 object classes. Both PCA and ICA are special cases of the Factor Analysis model, with different assumptions on the latent variables. Factor Analysis is a statistical model which can be used for revealing hidden factors that underlie a vector of random variables. In the case of CNN for image classification, the neurons or computational units in the output layer of a CNN, as random variables, represent object classes. A la-

tent factor might represent a common visual attribute shared by several object classes. It is therefore desirable to visualize, interpret and make use of the Factor Analysis models learned on the outputs of a trained CNN.

2. Softmax

Because a CNN was trained with one-hot hard targets (class labels), given a training image as input, the softmax function suppresses the outputs of most neurons in the output layer and leaves one or a few peak values. For example, in Figure 1 (a), we show the softmax ($T = 1$) outputs for a training image. To magnify the tiny values in the softmax outputs, after a CNN was trained with softmax function ($T = 1$), we take the logits \mathbf{y} in e.q. (1) and apply the following normalization function

$$x_i = \frac{(y_i - \min_k y_k)}{\sum_j (y_j - \min_k y_k)} \quad (2)$$

for all i , as the outputs of the CNN, with all the parameters in the CNN unchanged. This function normalizes \mathbf{y} so that \mathbf{x} in eq. (2) is still a probability distribution over classes. We call the \mathbf{x} in eq. (2) normalized logits. In Figure 1 (b), we show the outputs of this function given the same input image as Figure 1 (a).

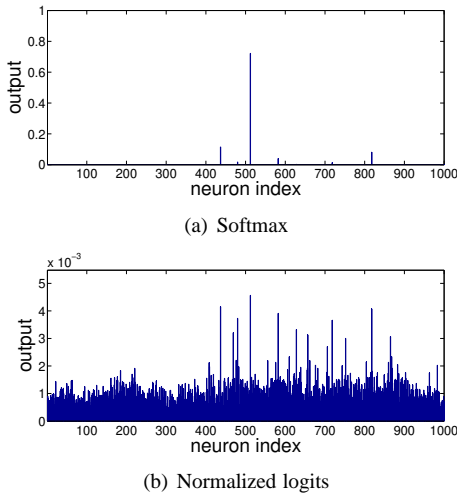


Figure 1. Outputs

In order to apply ICA, the variables must not all be Gaussian. The non-Gaussianity of a random variable x of zero mean can be measured by kurtosis $E(x^4)/E(x^2)^2 - 3$, which is zero if x is Gaussian. We computed the kurtosis of the outputs (mean removed) of a CNN with softmax and normalized logits using all the ImageNet ILSVRC2012 training data. The CNN model and experimental settings are described in Section 4. The result is, all neurons in the output layer have positive kurtosis, as shown in Figure 2.

Therefore the neurons as random variables are highly non-Gaussian and it is sensible to apply ICA, which is introduced in the next section.

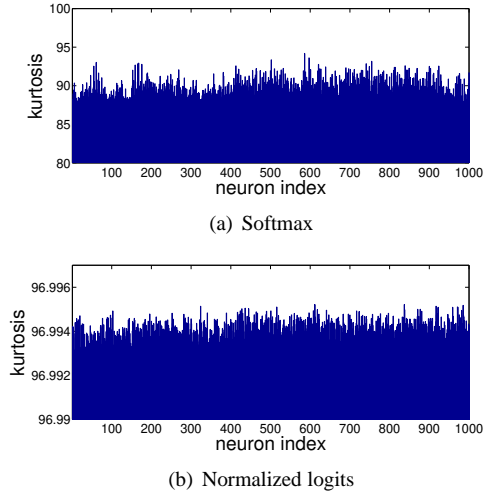


Figure 2. Kurtosis

3. Factor Analysis

In Factor Analysis, we assume the observed variables $\mathbf{x} = (x_1, \dots, x_n)$ are generated by the following model

$$\mathbf{x} = \mathbf{A}\mathbf{s} + \mathbf{n} \quad (3)$$

where $\mathbf{s} = (s_1, \dots, s_n)$ are the latent variables, \mathbf{A} is the model parameter matrix and \mathbf{n} are the noise variables. Here, \mathbf{x} and \mathbf{s} are assumed to have zero-mean. \mathbf{s} are also assumed to be uncorrelated and have unit variance, in other words, white.

3.1. Principle Component Analysis

Principle Component Analysis (PCA) is a special case of Factor Analysis. In PCA, \mathbf{s} are assumed to be Gaussian and \mathbf{n} are assumed to be zero (noise-free). Let \mathbf{C} denotes the covariance matrix of \mathbf{x} , $\mathbf{E} = (\mathbf{e}_1, \dots, \mathbf{e}_n)$ denotes the matrix of eigenvectors of \mathbf{C} and $\mathbf{D} = \text{diag}(\lambda_1, \dots, \lambda_n)$ denotes the diagonal matrix of eigenvalues of \mathbf{C} . The PCA matrix is \mathbf{E}^T , the whitening matrix is $\mathbf{U} = \mathbf{D}^{-1/2}\mathbf{E}^T$ and the whitened variables are $\mathbf{z} = \mathbf{U}\mathbf{x}$.

3.2. Independent Component Analysis

Independent Component Analysis (ICA) [20] is another special case of Factor Analysis. In ICA, \mathbf{s} are assumed to be non-Gaussian and independent and \mathbf{n} are assumed to be zero. ICA seeks a demixing matrix \mathbf{W} such that $\mathbf{W}\mathbf{x}$ can be as independent as possible. To obtain \mathbf{W} , we can first decompose it as $\mathbf{W} = \mathbf{V}\mathbf{U}$, where \mathbf{U} is the whitening matrix and \mathbf{V} is an orthogonal matrix, which can be learned by

maximizing the non-Gaussianity or the likelihood function of $\mathbf{V}\mathbf{U}\mathbf{x}$. The non-Gaussianity can be measured by kurtosis or negentropy. If dimensionality reduction is required, we can take the d largest eigenvalues and the corresponding eigenvectors for the whitening matrix \mathbf{U} . As a result, the size of \mathbf{U} is $d \times n$ and the size of \mathbf{V} is $d \times d$. ICA is ambiguous of scaling each component. If \mathbf{W} is an ICA demixing matrix, then $\text{diag}(\alpha_1, \dots, \alpha_d)\mathbf{W}$ is also an ICA demixing matrix, where $\{\alpha_1, \dots, \alpha_d\}$ are non-zero scaling constants of the components.

A classic ICA algorithm is FastICA [18]. Despite its fast convergence, FastICA is a batch algorithm which requires all the data to be loaded for computation in each iteration. Thus, it is unsuitable for large scale applications. To handle large scale datasets, we use a stochastic gradient descent (SGD) based ICA algorithm (described in the Appendix of [18] and Section 3.4 of [19]). For samples $\{\mathbf{z}(1), \mathbf{z}(2), \dots\}$, one updating step of the SGD-based algorithm of a given sample $\mathbf{z}(t)$ is:

$$\mathbf{V} \leftarrow \mathbf{V} + \mu g(\mathbf{V}\mathbf{z}(t))\mathbf{z}(t)^T + \frac{1}{2}(\mathbf{I} - \mathbf{V}\mathbf{V}^T)\mathbf{V}^T \quad (4)$$

where μ is the learning rate, $g(\cdot) = -\tanh(\cdot)$ and \mathbf{I} is an identity matrix. In our experiments, \mathbf{V} was initialized as a random orthogonal matrix.

Like FastICA, this SGD-based algorithm requires going through all data once to compute the whitening matrix \mathbf{U} . But unlike FastICA, this SGD-based algorithm does not require projection or orthogonalization in each step.

In this algorithm, the assumption on the probability distribution of each s_i is a super-Gaussian distribution

$$\log p(s_i) = -\log \cosh(s_i) + \text{constant} \quad (5)$$

and therefore

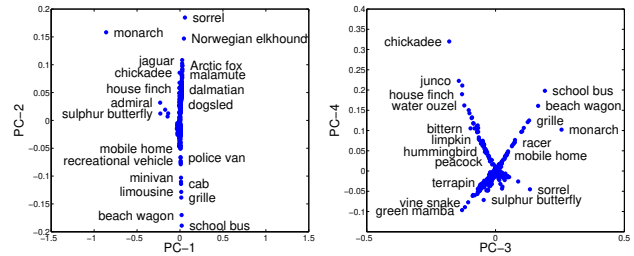
$$g(s_i) = \frac{\partial}{\partial s_i} \log p(s_i) = -\tanh(s_i). \quad (6)$$

Since the variables obtained by linear transformations of Gaussian variables are also Gaussian, from Section 2, we can infer that at least one neuron in the output layer is non-Gaussian. As an initial attempt, we choose a particular non-Gaussian distribution here. Explorations of different non-Gaussian distributions and therefore different nonlinearities $g(\cdot)$ are left for future research.

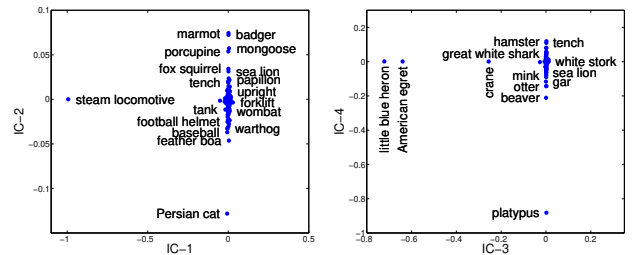
4. Results

4.1. Experimental Settings

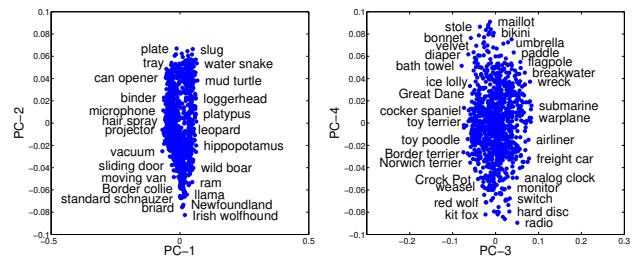
For the trained CNN model, we used GoogLeNet [35] and AlexNet [22]. The results of using two different CNN models are similar. Therefore, due to the space limitation, we only report the results of using GoogLeNet. We used



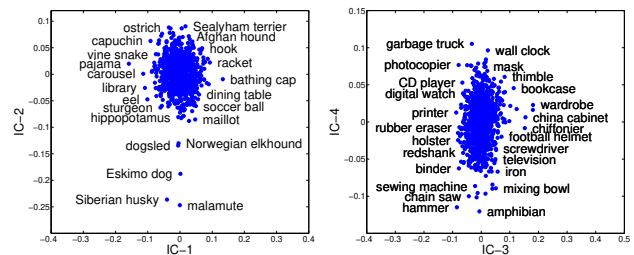
(a) PCA, softmax.



(b) ICA, softmax.



(c) PCA, normalized logits.



(d) ICA, normalized logits.

Figure 3. Label embedding of object class by PCA/ICA components. In each plot, each point is an object class and each axis is a PCA/ICA component (PC/IC). For visual clarity, only selected points are annotated with object class labels.

all the images in the ImageNet ILSVRC2012 training set to compute the ICA matrix using our SGD-based algorithm with mini-batch size 500. The learning rate was set to 0.005 and was halved every 10 epochs. The computation of CNN outputs was done with Caffe [21]. The ICA algorithm was ran with Theano [5].

Table 1. Object classes ranked by single components of PCA/ICA

	1	2	3	4
PCA	mosque shoji trimaran fire screen aircraft carrier	killer whale beaver valley otter loggerhead	Model T strawberry hay electric locomotive scoreboard	zebra tiger chickadee school bus yellow lady's slipper
ICA	mosque barn planetarium dome palace	killer whale grey whale dugong leatherback turtle sea lion	Model T car wheel tractor disk brake barn	zebra tiger triceratops prairie chicken warthog

4.2. Visualization of PCA/ICA components

To understand what is learned by PCA and ICA, we visualize the PCA and the ICA matrices. In the PCA matrix E^T or ICA matrix W , each row corresponds to a PCA/ICA component and each column corresponds to an object class. The number of rows depends on the dimensionality reduction. The number of columns of E^T or W is 1000, corresponding to 1000 classes. After the ICA matrix was learned, each ICA component (a row of W) was scaled to have unit l_2 norm. The scaling of each ICA component does not affect the ICA solution, as discussed in Section 3.2.

In Figure 3, we show the embedding of class labels by PCA and ICA. The horizontal and the vertical axes are two distinct rows of E^T or W . Each point in the plot corresponds to an object class. And there are 1000 points in each plot. Dimensionality is reduced from 1000 to 200 in ICA. In Figure 3 (a) and (b), we plot two pairs of the PCA/ICA components, learned with softmax outputs. In the PCA embedding, visually similar class labels are along some lines, but not the axes, while in the ICA embedding, they are along the axes. However, most points are clustered in the origin. In Figure 3 (c) and (d), we plot two pairs of the PCA/ICA components, learned with normalized logits outputs. We can see the class labels are more scattered in the plots.

In Figure 4, we show the PCA/ICA components of two sets of similar object classes: (1) *Border terrier*, *Lerry blue terrier*, and *Irish terrier*. (2) *trolleybus*, *minibus*, and *sports car*. Both PCA and ICA were learned on the softmax outputs and the dimensionality were reduced to 20 for better visualization. In Figure 4 (a), we see the PCA components of the object classes are distributed. While in Figure 4 (b), we see clearly that some single components of ICA are dominating. These components seem to represent "dog-ness" and "car-ness". Therefore, the ICA components are more interpretable.

In Table 1, we show the top-5 object classes according to the value of PCA/ICA components. For the ease of comparison, we selected each PCA/ICA component which has the largest value for class *mosque*, *killer whale*, *Model T* or *zebra* among all components. We can see that the class la-

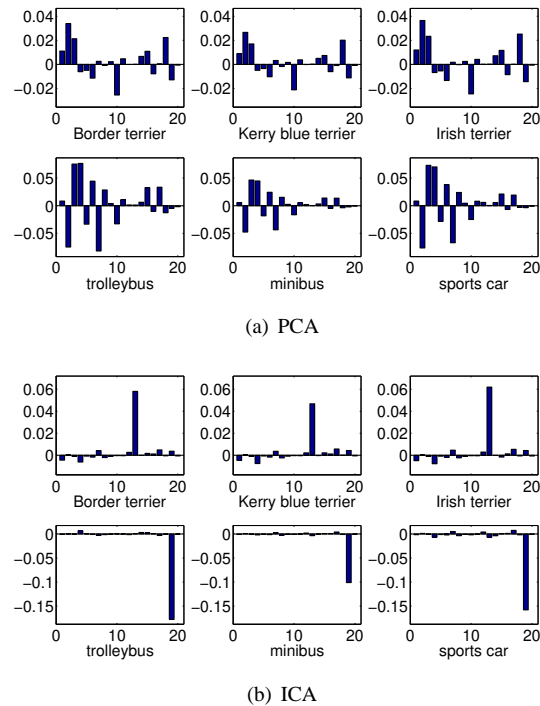


Figure 4. Bar plots of PCA/ICA components of object classes. Dimensionality was reduced to 20 for better visualization.

bels ranked by ICA components are more visually similar and consistent than the ones by PCA components.

The PCA/ICA components can be interpreted as common features shared by visually similar object classes. From Figure 3 and Table 1, we can see the label embeddings of object classes by PCA/ICA components are meaningful since visually similar classes are close in the embeddings. Unlike [1], these label embeddings can be unsupervisedly learned with a CNN trained with only one-hot class labels and without any hand annotated attribute label of the object classes, such as *has tail* or *lives in the sea*.

Table 2. Closest object classes in terms of visual and semantic similarity

	Egyptian cat	soccer ball	mushroom	red wine
Visual	tabby cat	rugby ball	bolete	wine bottle
	tiger cat	croquet ball	agaric	beer glass
	tiger	racket	stinkhorn	goblet
	lynx	tennis ball	earthstar	measuring cup
	Siamese cat	football helmet	hen-of-the-woods	wine bottle
Semantic	Persian cat	croquet ball	cucumber	eggnog
	tiger cat	golf ball	artichoke	cup
	Siamese cat	baseball	cardoon	espresso
	tabby cat	ping-pong ball	broccoli	menu
	cougar	punching bag	cauliflower	meat loaf

4.3. Visual vs. Semantic Similarity

The visual-semantic similarity relationship was previously explored in [9], which shows some consistency between two similarities. Here we further explore it from another perspective. We define the visual and the semantic similarity in the following way. The visual similarity between two object classes is defined as cosine similarity of their PCA or ICA components (200-dim and learned with softmax), both of which give the same results. The semantic similarity is defined based on the shortest path length¹ between two classes on the WordNet graph [12].

In Table 2, we compare five closest classes of *Egyptian cat*, *soccer ball*, *mushroom* and *red wine* in terms of visual and semantic similarities. For *Egyptian cat*, both visual and semantic similarities give similar results. For *soccer ball*, the visual similarity gives *football helmet* which is quite distant in terms of semantic similarities. For *mushroom* and *red wine*, two similarities give very different closest object classes. The gap between two similarities is intriguing and therefore worth further exploration. In neuroscience literature, it is claimed that visual cortex representation favors visual rather than semantic similarity [4].

5. Application: Zero-shot Learning

To demonstrate the effectiveness of the visual features of object classes learned by PCA and ICA, we apply them to zero-shot learning. Zero-shot learning [24, 23, 30, 31, 34] is a classification task in which some classes have no training data at all. We call the classes which have training data *seen classes* and those which have no training data *unseen classes*. One can use external knowledge of the classes, such as attributes, to build the relationship between the seen and the unseen classes. Then one can extrapolate the unseen classes by the seen classes.

Note that the focus of this paper is not zero-shot learning, but the visual features learned by PCA and ICA on the CNN

¹Computed with the `path_similarity()` function in the NLTK tool <http://www.nltk.org/howto/wordnet.html>.

outputs. Our purpose here is to give an example of how the learned PCA/ICA features can be used for computer vision applications. We intend to demonstrate the effectiveness of the PCA/ICA features compared to random features in large scale zero-shot learning experiments. However, we do not intend to provide a comprehensive comparison or review of different zero-shot learning methods.

5.1. Previous Work

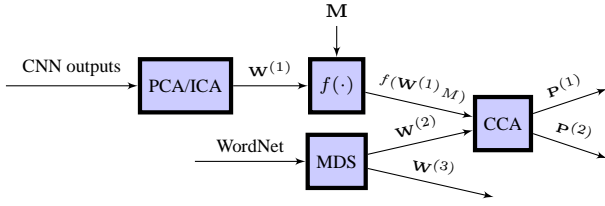
The current state-of-the-art large scale zero-shot learning methods are DeViSE [13] and conSE [29]. Both of them use the ImageNet of 1000 classes for training and the ImageNet of over 20000 classes for testing.

In DeViSE, a CNN is first pre-trained on the ImageNet of 1000 classes. Then, 500-dimensional semantic features of both seen and unseen classes are obtained by running Word2Vec [27] on Wikipedia. After that, the last (softmax) layer of the CNN is removed and all the other parts of the CNN are fine-tuned to predict the semantic features of the seen classes for each training image. In testing, when a new image arrives, the prediction is done by computing the cosine similarity of the CNN output vector and the semantic features of classes. In [13], it has also been shown that DeViSE could give more semantically reasonable errors for the seen classes.

In conSE, a CNN is first trained on the ImageNet of 1000 classes and 500-dimensional semantic features of the classes are obtained by running Word2Vec on Wikipedia, as in DeViSE. However, conSE does not require fine-tuning the CNN to predict the semantic features. The output vector in conSE is a convex combination of the semantic features, by the top activated neurons in the softmax layer. Its testing procedure is the same as DeViSE. In [29], it has been shown that conSE gives better performance than DeViSE in the large scale zero-shot learning experiments.

Our method differs from DeViSE and conSE by using unsupervised learning algorithms to learn: (1) visual features of classes. (2) a semantic features of classes from the WordNet graph, instead of Wikipedia. (3) a bridge between

Learning



Testing

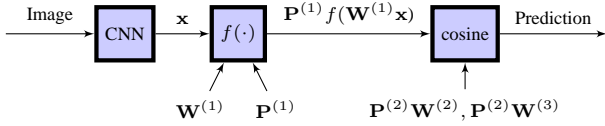


Figure 5. Our zero-shot learning method. $\mathbf{W}^{(1)}$ are the visual features of the seen classes. $\mathbf{W}^{(2)}$ are the semantic features of the seen classes. $\mathbf{W}^{(3)}$ are the semantic features of the unseen classes. $\mathbf{P}^{(1)}$ is the projection matrix from visual space to the common space. $\mathbf{P}^{(2)}$ is the projection matrix from semantic space to the common space. $f(\cdot)$ is the l_1 normalization. \mathbf{M} are the mean vectors of the seen classes. \mathbf{x} is the CNN output vector.

the visual and the semantic features.

5.2. Our Method

Our method works as follows. In the learning phase, first assume we have obtained the visual feature vectors $\mathbf{W}^{(1)} = (\mathbf{w}_1^{(1)}, \dots, \mathbf{w}_n^{(1)})$ of n seen classes. Let $\mathbf{M} = (\mathbf{m}_1, \dots, \mathbf{m}_n)$ denotes the matrix of the mean outputs of a CNN of the seen classes. And $\mathbf{F} = f(\mathbf{W}^{(1)}\mathbf{M}) = (\mathbf{f}_1, \dots, \mathbf{f}_n)$ are the transformed mean outputs of the seen classes, where $f(\cdot)$ is a nonlinear function. Next, assume we have obtained the semantic feature vectors $\mathbf{W}^{(2)} = (\mathbf{w}_1^{(2)}, \dots, \mathbf{w}_n^{(2)})$ of n seen classes and $\mathbf{W}^{(3)} = (\mathbf{w}_1^{(3)}, \dots, \mathbf{w}_m^{(3)})$ of m unseen classes. Due to the visual-semantic similarity gap shown in Section 4.3, we learn a bridge between the visual and the semantic representations of object classes via Canonical Correlation Analysis (CCA) [17, 15], which seeks two projection matrices $\mathbf{P}^{(1)}$ and $\mathbf{P}^{(2)}$ such that

$$\min_{\mathbf{P}^{(1)}, \mathbf{P}^{(2)}} \|\mathbf{P}^{(1)T}\mathbf{F} - \mathbf{P}^{(2)T}\mathbf{W}^{(2)}\|_F \quad (7)$$

$$\text{s.t. } \mathbf{P}^{(k)T}\mathbf{C}_{kk}\mathbf{P}^{(k)} = \mathbf{I}, \quad \mathbf{p}_i^{(k)T}\mathbf{C}_{kl}\mathbf{p}_j^{(l)} = 0, \quad (8)$$

$$k, l = 1, 2, \quad k \neq l, \quad i, j = 1, \dots, d, \quad (9)$$

where $\mathbf{p}_i^{(k)}$ is the i -th column of $\mathbf{P}^{(k)}$ and \mathbf{C}_{kl} is a covariance or cross-covariance matrix of $\{\mathbf{f}_1, \dots, \mathbf{f}_n\}$ and/or $\{\mathbf{w}_1^{(2)}, \dots, \mathbf{w}_n^{(2)}\}$.

In the testing phase, when a new image arrives, we first compute its CNN output \mathbf{x} . Then for $\mathbf{P}^{(1)T}(f(\mathbf{W}^{(1)}\mathbf{x}) -$

$\frac{1}{n} \sum_i \mathbf{f}_i)$, we compute its k closest columns of $\mathbf{P}^{(2)T}\mathbf{W}^{(2)}$ (seen) and/or $\mathbf{P}^{(2)T}\mathbf{W}^{(3)}$ (unseen). The corresponding classes of these k columns are the top- k predictions. The closeness is measured by cosine similarity.

For $\mathbf{W}^{(1)}$, we compare random, PCA, and ICA matrices of different dimensionality in our experiments. The random matrices are semi-orthogonal, that is, $\mathbf{W}^{(1)}\mathbf{W}^{(1)T} = \mathbf{I}$ but $\mathbf{W}^{(1)}\mathbf{W}^{(1)T} \neq \mathbf{I}$. For $\mathbf{W}^{(2)}$ and $\mathbf{W}^{(3)}$, we use the feature vectors by running classic Multi-dimensional Scaling (MDS) on a distance matrix of both seen and unseen classes. The distance between two classes is measured by one minus the similarity in Section 4.3. Each column of $\mathbf{W}^{(2)}$ and $\mathbf{W}^{(3)}$ is subtracted by $\frac{1}{n} \sum_i \mathbf{w}_i^{(2)}$. \mathbf{M} is approximated by \mathbf{I} and $f(\cdot)$ is the scaling normalization of a vector or each column of a matrix to unit l_1 norm. We experimented with softmax with different T and normalized logits as the outputs. The best performance (as in Table 4, 3, 5) was obtained with the softmax ($T = 1$) output for \mathbf{x} but \mathbf{E}^T and \mathbf{W} were learnt with normalized logits.

We use a new and simple method for obtaining the semantic features of classes, MDS on WordNet. Compare to Word2Vec on Wikipedia, this avoid three problems: (1) Word ambiguity. There are words which have multiple meanings and represent multiple classes. For example, there are two classes in ImageNet both named *fly*. One means the insect and the other means the fishermen’s lure. (2) Multiple annotations. There are several classes which have multiple annotations. For example, class *lesser panda*, *red panda*, *panda*, *bear cat*, *cat bear*, *Ailurus fulgens*. With Word2Vec on Wikipedia, one would obtain multiple feature vectors for these classes. This is no principled way of selecting or combining them. (3) Heavy computation. Typically, Word2Vec on Wikipedia consumes a large amount of RAM and takes hours for computation. While classic MDS on the WordNet distance matrix of size 21842×21842^2 is much cheaper to compute. The computation of a 21632-dimensional MDS feature vector for each class was done in MATLAB with 8 Intel Xeon 2.5GHz cores within 12 minutes. A comparison of different semantic features of classes for zero-shot learning can be found in [2]. However, MDS on WordNet was not compared in [2] (only the raw WordNet distance matrix) and is a part of the contribution of this paper.

5.3. Experiments

Following the zero-shot learning experimental settings of DeViSE and conSE, we used a CNN trained on ImageNet ILSVRC2012 (1000 seen classes), and test our method to classify images in ImageNet 2011fall (20842 unseen

²21841 classes in ImageNet 2011fall plus class *teddy*, *teddy bear*. Class *teddy*, *teddy bear* (WordNet ID: n04399382) is in ImageNet ILSVRC2012 but not in ImageNet 2011fall.

classes³, 21841 both seen and unseen classes). We use top- k accuracy (also called flat hit@ k in [13, 29]) measure, the percentage of test images in which a method’s top- k predictions return the true label. The code for the experiments can be downloaded in⁴.

For the trained CNN model, we experimented with GoogLeNet and AlexNet. Although GoogLeNet outperforms AlexNet on the seen classes, two CNN models in our method perform essentially the same on the zero-shot learning tasks. Due to the space limitation, we only report the results of using GoogLeNet.

The sizes of the matrices in our methods: $\mathbf{W}^{(1)}$ is $k \times 1000$, $\mathbf{W}^{(2)}$ is 21632×1000 , $\mathbf{W}^{(3)}$ is 21632×20842 , $\mathbf{P}^{(1)}$ is $k \times k$, $\mathbf{P}^{(2)}$ is $k \times 21632$, \mathbf{M} is 1000×1000 and \mathbf{x} is 1000×1 . We used $k = 100, 500, 900$ in our experiments. Although $\mathbf{W}^{(2)}$ and $\mathbf{W}^{(3)}$ are large matrices, we only need to compute once and store $\mathbf{P}^{(2)}\mathbf{W}^{(2)}$ and $\mathbf{P}^{(2)}\mathbf{W}^{(3)}$ of size $k \times 1000$ and $k \times 21632$, respectively.

In Table 3, we show the results of the three zero-shot learning methods on the test images selected in [29]. Same as conSE, our method gives correct or reasonable predictions.

In Table 4, we show the results of different methods on ImageNet 2011fall. Our method performs better when using PCA or ICA for the visual features than random features. And our method, especially with PCA or ICA features, achieves superior results on this zero-shot learning task.

In Table 5, we show the results of different methods on ImageNet ILSVRC2012 validation set of 1000 seen classes. While the goal here is not to classify images of seen classes, it is desirable to measure how much accuracy a zero-shot learning method would lose compared to the softmax baseline. Again, we can see that our method performs better using PCA or ICA for the visual features than random features.

The results show that in our method the PCA or ICA matrix as visual features of object classes performs better than a random matrix. Therefore, these visual features, learned PCA and ICA on the outputs of CNN, are indeed effective for the subsequent tasks. The results also show that PCA and ICA give the essentially same classification accuracy. Therefore, in practice we can use PCA instead of ICA, which has much higher computational costs. A comprehensive discussion on PCA vs. ICA for recognition tasks can be found in [3].

6. Discussions

The outputs of a neural network contains rich information. It has been claimed that one can determine a neu-

³Since class *teddy*, *teddy bear* is missing in ImageNet 2011fall, the correct number of classes is $21841 - (1000 - 1) = 20842$ rather than 20841.

⁴<https://github.com/yaolubrain/ULNNO>

ral network architecture from its outputs given arbitrary inputs [11]. Also, it has been shown that one can reconstruct the whole image to some degree with only its CNN outputs [10]. And smooth regularization on the output distribution of a neural network can help in reducing generalization error in both supervised and semi-supervised settings [28].

CNN achieves the state-of-the-art results on many computer vision tasks such as image classification and object detection. However, despite many efforts of visualizing and understanding CNN [37, 33, 38], it still reminds a black-box method. In this paper, we attempted to understand CNN by unsupervised learning. CNN was trained with only one-hot targets, which means we assumed object classes are equally similar. The CNN was never informed which classes more similar. However, unsupervised learning on CNN outputs reveals the visual similarity of object classes. We hope this finding can shed some lights on the object representation in CNN.

We also showed that there is a gap between the visual similarity of object classes in CNN and the semantic similarity of object classes in our knowledge graph WordNet. Therefore, a bridge should be built, in order to achieve consistent mapping between visual and semantic representations.

Supervised learning alone cannot deal with unseen classes since there is no training data. By using external knowledge and unsupervised learning algorithms, we can leverage supervised learning so as to make reasonable predictions on the unseen classes while maintaining the compatibility with the seen classes, that is, zero-shot learning. In this paper, we proposed a new zero-shot learning method, which achieves the state-of-the-art results on the ImageNet of over 20000 classes.

Acknowledgements

Yao Lu thanks his supervisors Aapo Hyvarinen and Michael Gutmann for their kind guidance. He also thanks Yoshua Bengio for an inspiring conversation on unsupervised learning and Kyunghyun Cho for helpful comments on the paper.

References

- [1] Z. Akata, F. Perronnin, Z. Harchaoui, and C. Schmid. Label-embedding for attribute-based classification. *CVPR*, 2013.
- [2] Z. Akata, S. Reed, D. Walter, H. Lee, and B. Schiele. Evaluation of output embeddings for fine-grained image classification. In *CVPR*, 2015.
- [3] M. Asuncion Vicente, P. O. Hoyer, and A. Hyvärinen. Equivalence of some common linear feature extraction techniques for appearance-based object recognition tasks. *TPAMI*, 2007.
- [4] C. Baldassi, A. Alemi-Neissi, M. Pagan, J. J. DiCarlo, R. Zecchina, and D. Zoccolan. Shape similarity, better than semantic membership, accounts for the structure of visual

Table 3. Predictions of test images of unseen classes (correct class labels are in blue)

Test Images	DeViSE [13]	ConSE [29]	Our Method
	water spaniel tea gown bridal gown, wedding gown spaniel tights, leotards	business suit dress, frock hairpiece, false hair, postiche swimsuit, swimwear, bathing suit kit, outfit	periwig, peruke horsehair wig hound, hound dog bonnet macaque toupee, toupe
	heron owl, bird of Minerva, bird of night hawk bird of prey, raptor, raptorial bird finch	ratite, ratite bird, flightless bird peafowl, bird of Juno common spoonbill New World vulture, cathartid Greek partridge, rock partridge	ratite, ratite bird, flightless bird kiwi, apteryx moa elephant bird, aepyornis emu, Dromaius novaehollandiae
	elephant turtle turtleneck, turtle, polo-neck flip-flop, thong handcart, pushcart, cart, go-cart	California sea lion Steller sea lion Australian sea lion South American sea lion eared seal	fur seal ^a eared seal fur seal ^b guadalupe fur seal Alaska fur seal
	golden hamster, Syrian hamster rhesus, rhesus monkey pipe shaker American mink, Mustela vison	golden hamster, Syrian hamster rodent, gnawer Eurasian hamster rhesus, rhesus monkey rabbit, coney, cony	golden hamster, Syrian hamster Eurasian hamster prairie dog, prairie marmot skink, scincid, scincid lizard mountain skink
	truck, motortruck skidder tank car, tank automatic rifle, machine rifle trailer, house trailer	flatcar, flatbed, flat truck, motortruck tracked vehicle bulldozer, dozer wheeled vehicle	farm machine cultivator, tiller skidder bulldozer, dozer haymaker, hay conditioner
	kernel littoral, littoral, littoral zone, sands carillon Cabernet, Cabernet Sauvignon poodle, poodle dog	dog, domestic dog domestic cat, house cat schnauzer Belgian sheepdog domestic llama, Lama peruana	mastiff alpaca, Lama pacos domestic llama, Lama peruana guanaco, Lama guanicoe Seeing Eye dog

Table 4. Top-*k* accuracy in ImageNet 2011 fall zero-shot learning task (%)

Test Set	#Classes	#Images	Method	Top-1	Top-2	Top-5	Top-10	Top-20
Unseen	20842	12.9 million	DeViSE (500-dim)	0.8	1.4	2.5	3.9	6.0
			ConSE (500-dim)	1.4	2.2	3.9	5.8	8.3
			Our method (100-dim, random)	1.4	2.2	3.4	4.3	5.2
			Our method (100-dim, PCA)	1.6	2.7	4.6	6.4	8.6
			Our method (100-dim, ICA)	1.6	2.7	4.6	6.3	8.5
			Our method (500-dim, random)	1.8	2.9	5.0	6.9	8.8
			Our method (500-dim, PCA)	1.8	3.0	5.2	7.3	9.6
			Our method (500-dim, ICA)	1.8	3.0	5.2	7.3	9.7
			Our method (900-dim, random)	1.8	3.0	5.1	7.2	9.6
			Our method (900-dim, PCA)	1.8	3.0	5.2	7.3	9.7
Our method (900-dim, ICA)	1.8	3.0	5.2	7.3	9.7			
Both	21841	14.2 million	DeViSE (500-dim)	0.3	0.8	1.9	3.2	5.3
			ConSE (500-dim)	0.2	1.2	3.0	5.0	7.5
			Our method (100-dim, random)	6.7	8.2	10.0	11.1	12.1
			Our method (100-dim, PCA)	6.7	8.1	10.3	12.4	14.8
			Our method (100-dim, ICA)	6.7	8.1	10.4	12.4	14.7
			Our method (500-dim, random)	6.7	8.5	11.2	13.4	15.6
			Our method (500-dim, PCA)	6.7	8.5	11.4	13.7	16.3
			Our method (500-dim, ICA)	6.7	8.5	11.4	13.7	16.3
			Our method (900-dim, random)	6.7	8.5	11.4	13.7	16.2
			Our method (900-dim, PCA)	6.7	8.5	11.4	13.7	16.3
Our method (900-dim, ICA)	6.7	8.5	11.4	13.7	16.3			

^aWordNet ID: n02077152. There are two classes named *fur seal* with different WordNet IDs.

^bWordNet ID: n02077658.

Table 5. Top- k accuracy in ImageNet ILSVRC2012 validation set (%)

Test Set	#Classes	#Images	Method	Top-1	Top-2	Top-5	Top-10	Top-20
Seen	1000	50000	Softmax baseline (1000-dim)	55.6	67.4	78.5	85.0	-
			DeViSE (500-dim)	53.2	65.2	76.7	83.3	-
			ConSE (500-dim)	54.3	61.9	68.0	71.6	-
			Our softmax baseline (1000-dim)	67.1	78.8	87.9	92.2	95.2
			Our method (100-dim, random)	67.0	74.6	77.8	79.1	80.4
			Our method (100-dim, PCA)	67.0	76.9	84.6	88.5	91.5
			Our method (100-dim, ICA)	67.0	76.9	84.6	88.5	91.5
			Our method (500-dim, random)	67.1	77.3	83.5	85.4	86.6
			Our method (500-dim, PCA)	67.1	78.2	86.2	89.4	91.2
			Our method (500-dim, ICA)	67.1	78.2	86.2	89.3	91.2
			Our method (900-dim, random)	67.1	78.3	86.0	88.6	90.1
			Our method (900-dim, PCA)	67.1	78.5	86.6	89.8	91.7
			Our method (900-dim, ICA)	67.1	78.4	86.5	89.8	91.7

object representations in a population of monkey inferotemporal neurons. *PLoS computational biology*, 2013.

- [5] J. Bergstra, O. Breuleux, F. Bastien, P. Lamblin, R. Pascanu, G. Desjardins, J. Turian, D. Warde-Farley, and Y. Bengio. Theano: a CPU and GPU math expression compiler. *SciPy*, 2010.
- [6] C. F. Cadieu, H. Hong, D. L. Yamins, N. Pinto, D. Ardila, E. A. Solomon, N. J. Majaj, and J. J. DiCarlo. Deep neural networks rival the representation of primate it cortex for core visual object recognition. *PLoS computational biology*, 2014.
- [7] D. Ciresan, U. Meier, and J. Schmidhuber. Multi-column deep neural networks for image classification. *CVPR*, 2012.
- [8] J. Deng, W. Dong, R. Socher, L.-J. Li, K. Li, and L. Fei-Fei. Imagenet: A large-scale hierarchical image database. *CVPR*, 2009.
- [9] T. Deselaers and V. Ferrari. Visual and semantic similarity in imagenet. *CVPR*, 2011.
- [10] A. Dosovitskiy and T. Brox. Inverting convolutional networks with convolutional networks. *arXiv:1506.02753*, 2015.
- [11] C. Fefferman and S. Markel. Recovering a feed-forward net from its output. In *NIPS*, 1994.
- [12] C. Fellbaum. *WordNet: An Electronic Lexical Database*. 1998.
- [13] A. Frome, G. S. Corrado, J. Shlens, S. Bengio, J. Dean, T. Mikolov, et al. Devise: A deep visual-semantic embedding model. *NIPS*, 2013.
- [14] R. Girshick, J. Donahue, T. Darrell, and J. Malik. Rich feature hierarchies for accurate object detection and semantic segmentation. *CVPR*, 2014.
- [15] D. Hardoon, S. Szedmak, and J. Shawe-Taylor. Canonical correlation analysis: An overview with application to learning methods. *Neural computation*, 2004.
- [16] G. E. Hinton, O. Vinyals, and J. Dean. Distilling the knowledge in a neural network. *NIPS Deep Learning Workshop*, 2014.
- [17] H. Hotelling. Relations between two sets of variates. *Biometrika*, 1936.
- [18] A. Hyvarinen. Fast and robust fixed-point algorithms for independent component analysis. *TNN*, 1999.
- [19] A. Hyvarinen. Sparse code shrinkage: Denoising of non-gaussian data by maximum likelihood estimation. *Neural computation*, 1999.
- [20] A. Hyvärinen, J. Karhunen, and E. Oja. *Independent component analysis*. 2004.
- [21] Y. Jia, E. Shelhamer, J. Donahue, S. Karayev, J. Long, R. Girshick, S. Guadarrama, and T. Darrell. Caffe: Convolutional architecture for fast feature embedding. *arXiv:1408.5093*, 2014.
- [22] A. Krizhevsky, I. Sutskever, and G. E. Hinton. Imagenet classification with deep convolutional neural networks. *NIPS*, 2012.
- [23] C. H. Lampert, H. Nickisch, and S. Harmeling. Learning to detect unseen object classes by between-class attribute transfer. *CVPR*, 2009.
- [24] H. Larochelle, D. Erhan, and Y. Bengio. Zero-data learning of new tasks. *AAAI*, 2008.
- [25] Y. LeCun, L. Bottou, Y. Bengio, and P. Haffner. Gradient-based learning applied to document recognition. *Proceedings of the IEEE*, 1998.
- [26] J. Long, E. Shelhamer, and T. Darrell. Fully convolutional networks for semantic segmentation. *CVPR*, 2015.
- [27] T. Mikolov, K. Chen, G. Corrado, and J. Dean. Efficient estimation of word representations in vector space. *ICLR*, 2013.
- [28] T. Miyato, S.-i. Maeda, M. Koyama, K. Nakae, and S. Ishii. Distributional smoothing with virtual adversarial training. *arXiv:1507.00677*, 2015.
- [29] M. Norouzi, T. Mikolov, S. Bengio, Y. Singer, J. Shlens, A. Frome, G. S. Corrado, and J. Dean. Zero-shot learning by convex combination of semantic embeddings. *ICLR*, 2014.
- [30] M. Palatucci, D. Pomerleau, G. E. Hinton, and T. M. Mitchell. Zero-shot learning with semantic output codes. *NIPS*, 2009.
- [31] M. Rohrbach, M. Stark, and B. Schiele. Evaluating knowledge transfer and zero-shot learning in a large-scale setting. In *CVPR*, 2011.
- [32] R. G. J. S. Shaoqing Ren, Kaiming He. Faster R-CNN: Towards real-time object detection with region proposal networks. *NIPS*, 2015.

- [33] K. Simonyan, A. Vedaldi, and A. Zisserman. Deep inside convolutional networks: Visualising image classification models and saliency maps. *ICLR*, 2014.
- [34] R. Socher, M. Ganjoo, C. D. Manning, and A. Ng. Zero-shot learning through cross-modal transfer. In *NIPS*, 2013.
- [35] C. Szegedy, W. Liu, Y. Jia, P. Sermanet, S. Reed, D. Anguelov, D. Erhan, V. Vanhoucke, and A. Rabinovich. Going deeper with convolutions. *CVPR*, 2015.
- [36] S. C. Turaga, J. F. Murray, V. Jain, F. Roth, M. Helmstaedter, K. Briggman, W. Denk, and H. S. Seung. Convolutional networks can learn to generate affinity graphs for image segmentation. *Neural Computation*, 2010.
- [37] M. D. Zeiler and R. Fergus. Visualizing and understanding convolutional networks. *ECCV*, 2014.
- [38] B. Zhou, A. Khosla, A. Lapedriza, A. Oliva, and A. Torralba. Object detectors emerge in deep scene cnns. *ICLR*, 2015.